

X-ray fluorescence holography: beyond the diffraction limit

S. Marchesini¹ and C. S. Fadley^{1,2}

¹Materials Sciences Division, Lawrence Berkeley National Laboratory, Berkeley, California 94720

²Department of Physics, University of California, Davis, California 95616

(Dated: December 2, 2024)

Holography with inside source or inside detector is a method to obtain diffraction-limited images of atomic clusters. The reconstructed wave-field represents a distorted image of the scatterer density distribution, i.e. the convolution of the charge density distribution with a point spread function. We present several methods for the iterative deconvolution of inside source holograms.

PACS numbers: 61.14.-x, 42.40.-i

I. INTRODUCTION

X-ray fluorescence holography is a fascinating method to image the local environment of atomic species in oriented systems^{1,2,3}. When an atom inside an atomic cluster emits a spherical wave, the interference between the outgoing unperturbed wave and the scattered object wave represents the hologram. The holographic reconstruction is achieved by propagating back the wave-field from the far field.

Beyond the recent achievements of the methods⁴ another step toward the practical application of holography would be a quantitative link between the electronic charge distribution and the holographic image. The reconstructed wave-field can be viewed as a distorted image of the scatterer density distribution, i.e. the convolution of the charge density distribution with a point spread function.

When an object scene is imaged through an optical system, information is lost whenever the imaging system cannot pass all the spatial frequencies contained in the scene. Further loss is produced by aberrations in the optical system. The question that we address is how much information can be recovered if we know the point spread function (PSF) of the optical system.

Several methods for the iterative deconvolution have been developed in the field of astronomy and microscopy. The first method has been developed by Van Cittert in 1920⁵ using a self-consistent iterative solution to the problem. It can be shown that this method is close to the gradient search of the maximum likelihood (ML). Two other approaches are based on the probability theory. One developed by Lucy⁶ and Richardson⁷ is based on Bayes theorem for conditional probability. Another one, the maximum entropy method (MEM) seeks the ‘most probable’ solution in an under-determined system of equations.

In this article, we review some of these methods and report the first deconvolved atomic image at super resolution.

Consider a charge density distribution $\rho(\mathbf{r})$. Neglecting absorption the hologram χ in the far field \mathbf{k} is given by⁸:

$$\begin{aligned}\chi(\mathbf{k}) &= \int \eta(\mathbf{k}, \mathbf{r}) \rho(\mathbf{r}) d^3\mathbf{r}, \\ \eta(\mathbf{k}, \mathbf{r}) &= 2\text{Re} \left[\frac{r_e}{r} e^{i(kr - \mathbf{k} \cdot \mathbf{r})} f(\mathbf{k}, \mathbf{r}) \right];\end{aligned}\quad (1)$$

where r_e is the classical electron radius, $r_e f(\mathbf{k}, \mathbf{r})$ is the scattering factor per electron and the phase factor is the path length difference between the wave emitted from the origin and the wave scattered by the electron located in \mathbf{r} . The typical reconstruction algorithm to calculate the wavefield U in the real space \mathbf{r} is:

$$\begin{aligned}U(\mathbf{r}') &= \int_s \eta^{\{-1\}}(\mathbf{r}', \mathbf{k}) \chi(\mathbf{k}) d^3\mathbf{k}, \\ \eta^{\{-1\}}(\mathbf{r}', \mathbf{k}) &= \frac{r'}{r_e} e^{-i(kr' - \mathbf{k} \cdot \mathbf{r}')}\end{aligned}\quad (2)$$

where s is the measured region in \mathbf{k} -space. Sometimes⁹ an additional factor $f^{\{-1\}}$ is included to compensate the ‘aberration’ or distortions produced in the hologram χ by f . The holographic reconstruction U is a distorted image of the charge density distribution ρ :

$$\begin{aligned}U(\mathbf{r}') &= \int \mu(\mathbf{r}', \mathbf{r}) \rho(\mathbf{r}) d^3\mathbf{r}, \\ \mu(\mathbf{r}', \mathbf{r}) &= \int_s d^3\mathbf{k} \eta^{\{-1\}}(\mathbf{r}', \mathbf{k}) \eta(\mathbf{k}, \mathbf{r})\end{aligned}\quad (3)$$

here $\mu(\mathbf{r}', \mathbf{r})$ is the experimental point spread function. If we enforce the fact that the charge distribution is real, we need to use $\text{Re} \mu(\mathbf{r}', \mathbf{r})$.

In summary we have three spaces \mathbf{r} , \mathbf{k} and \mathbf{r}' for which we have three functions $\rho(\mathbf{r})$, $\chi(\mathbf{k})$ and $U(\mathbf{r}')$ and the propagators from one space to the other are $\eta(\mathbf{k}, \mathbf{r})$, $\eta^{\{-1\}}(\mathbf{k}, \mathbf{r}')$ and $\mu(\mathbf{r}', \mathbf{r})$.

In the following sections the symbol $*$ between two functions stands for the integration over the internal variable, e.g. $f(x, y) * g(y) = \int dy f(x, y)g(y)$.

II. ITERATIVE IMAGE DECONVOLUTION

The general problem of the deconvolution is to obtain the unknown object $\rho(\mathbf{r})$ from the knowledge of $U(\mathbf{r}')$ and $\mu(\mathbf{r}', \mathbf{r})$. The first method developed by Van Cittert in 1920⁵ is the most intuitive one and it is based on a self-consistent solution. Every step is the difference between the reconstructed experimental hologram $U(\mathbf{r})$ and the

reconstructed simulated hologram $U^{\{n\}}(\mathbf{r}) = \mu(\mathbf{r}, \mathbf{r}') * \rho^{\{n\}}(\mathbf{r})$ generated by the new charge density distribution.

$$\begin{aligned}\rho^{\{n+1\}}(\mathbf{r}) &= \rho^{\{n\}}(\mathbf{r}) + \Delta\rho^{\{n\}}(\mathbf{r}), \\ \Delta\rho^{\{n\}}(\mathbf{r}) &= [U(\mathbf{r}) - U^{\{n\}}(\mathbf{r}')], \\ \rho^{\{1\}}(\mathbf{r}) &= U(\mathbf{r}).\end{aligned}\quad (4)$$

A similar problem is the phase retrieval of a diffraction pattern of known intensity from an object with known support $s(\mathbf{r})$. If the object is constrained within a given support, the product of the object $\rho(\mathbf{r})$ with the support function $s(\mathbf{r})$ must be still equal to the object. Therefore the complex amplitude of the diffracted wave-field is not modified by a convolution with the Fourier transform of the support function, *i.e.* $\tilde{\rho} = \tilde{s} * \tilde{\rho}$. If \tilde{s} is sufficiently large (over-sampling condition¹⁰) a certain number of pixels are bounded by the self-consistent equation. The main difference with iterative deconvolution methods is that in this case, the bigger is \tilde{s} the better. In such case, iterative approaches such as the Gerchberg-Saxton¹¹ and Fienup¹² algorithms can solve the phase problem. In the Fourier domain the Gerchberg-Saxton algorithm can be expressed as:

$$\tilde{\rho}^{\{n+1\}} = \frac{\tilde{\rho}^{\{n\}} * \tilde{s}}{|\tilde{\rho}^{\{n\}} * \tilde{s}|} \quad |\tilde{\rho}_{\text{exp}}| = |\tilde{\rho}_{\text{exp}}| e^{i \text{phase}\{\tilde{\rho}^{\{n\}} * \tilde{s}\}}$$

Another approach is given by the Lucy-Richardson method^{6,7}. This method is based on a self-consistent iterative solution of the Bayes theorem for conditional probabilities, considering $\mu(\underline{\mathbf{r}}, \underline{\mathbf{r}})$ as a probability that \mathbf{r}' will fall in the interval $(\underline{\mathbf{r}}, \underline{\mathbf{r}} + d\underline{\mathbf{r}})$ when it is known that $\mathbf{r} = \underline{\mathbf{r}}$. A self-consistent iterative approach can be expressed as⁶:

$$\begin{aligned}\rho^{\{n+1\}}(\mathbf{r}) &= \rho^{\{n\}}(\mathbf{r}) \\ &\times \left[\mu^T(\mathbf{r}, \mathbf{r}') * \frac{U(\mathbf{r}')}{\mu(\mathbf{r}', \mathbf{r}'') * \rho^{\{n\}}(\mathbf{r}'')} \right]\end{aligned}\quad (5)$$

III. MAXIMUM LIKELIHOOD AND ENTROPY

We want to minimize the difference between the measured hologram in the far field $\chi(\mathbf{k})$ and the hologram generated by a given charge density distribution $\rho^{\{n\}}(\mathbf{r})$:

$$Q = \int_s d^3\mathbf{k} \left| \chi(\mathbf{k}) - \eta(\mathbf{k}, \mathbf{r}) * \rho^{\{n\}}(\mathbf{r}) \right|^2 \quad (6)$$

where the unknowns are $\rho^{\{n\}}(\mathbf{r}_i)$, $i = 1 \dots N$. The gradient can be computed as:

$$\nabla Q = 2\eta^\dagger(\mathbf{r}, \mathbf{k}) * \left[\eta(\mathbf{k}, \mathbf{r}) * \rho^{\{n\}}(\mathbf{r}) - \chi(\mathbf{k}) \right] \quad (7)$$

The Hessian is:

$$\begin{aligned}H &= \frac{\partial^2 Q}{\partial \rho^{\{n\}}(\mathbf{r}_1) \partial \rho^{\{n\}}(\mathbf{r}_2)} \\ &= 2\eta^\dagger(\mathbf{r}_1, \mathbf{k}) * \eta(\mathbf{k}, \mathbf{r}_2)\end{aligned}\quad (8)$$

The single pixel approximation^{13,14} consists in assuming that H is diagonal, so that the steps will be:

$$\Delta\rho^{\{n\}}(\mathbf{r}) = -\frac{1}{H_{\mathbf{r}, \mathbf{r}}} \nabla Q_r \quad (9)$$

Under this approximation, the gradient search is equivalent to the Van Cittert method, since $H_{\mathbf{r}, \mathbf{r}} \simeq \left(\frac{r_e}{r}\right)^2$ (see appendix A) and $\eta^{\{-1\}} = \frac{r^2}{r_e^2} \eta^\dagger$. For single energy holograms, at the symmetric position to the real atoms, appears a twin or ghost image. Therefore one should consider at least the symmetric term $H_{\mathbf{r}, -\mathbf{r}}$:

$$\bar{H}_{\mathbf{r}, \mathbf{r}'} = H_{\mathbf{r}, \mathbf{r}'} (\delta_{\mathbf{r}', \mathbf{r}} + \delta_{\mathbf{r}', -\mathbf{r}}) \quad (10)$$

$$\Delta\rho^{\{n\}}(\mathbf{r}) = -(\bar{H}_{\mathbf{r}, \mathbf{r}}^{-1} \nabla Q_{\mathbf{r}} + \bar{H}_{\mathbf{r}, -\mathbf{r}}^{-1} \nabla Q_{-\mathbf{r}}) \quad (11)$$

however at every energy, for a given position, and in case of a point scattering the twin image cancels the real image, there is a divergence in equation (8). This can be avoided by introducing an anisotropy in the scattering factor. It is known¹⁵ that if we use small Gaussian charge distribution for every point \mathbf{r}_i instead of point scatterers, the scattering factor becomes anisotropic and iterative algorithms converge more quickly. Conjugate gradient methods do not require the calculation of the Hessian, but partial knowledge of it is helpful. Extra information can be used, we know that the scattering distribution is real and positive. This can be enforced by taking the real part at every step and by setting to $\rho_n = 0$ when $\rho_n(\mathbf{r}) < 0$. Further extra information is the total number of scattering electrons, and we can use Lagrange multipliers to perform constrained best fit:

$$\begin{aligned}Q + \beta F, \\ F = \sum \rho(\mathbf{r}_i),\end{aligned}\quad (12)$$

the minimization is performed adjusting the multiplier β at every step:

$$\begin{aligned}\Delta\rho_{\mathbf{r}} &= -\bar{H}_{\mathbf{r}, \mathbf{r}'}^{-1} (\nabla Q_{\mathbf{r}'} + \beta \nabla F_{\mathbf{r}}), \\ \beta &= \frac{[F_0 - F + (\nabla F \cdot \bar{H}^{-1} \cdot \nabla Q)]}{\nabla F \cdot \bar{H}^{-1} \cdot \nabla F}\end{aligned}\quad (13)$$

The deconvolution of spectra with incomplete Fourier image is often treated with the maximum entropy method. When the number of unknowns $\rho(\mathbf{r}_i)$ is superior to the number of equations, it is necessary to include further a-posteriori information. As more than one solution

can satisfy the set of equation, we seek the most probable solution, i.e. the one with the maximum Entropy. In practice we want to minimize the functional:

$$Q + S, \quad S = \lambda \sum_i \rho(\mathbf{r}_i) \ln \rho(\mathbf{r}_i) \quad (14)$$

where λ is a Lagrange multiplier.

The procedure is similar to the previous one, with two main differences: (I) MEM enforces positivity, so that a pure gradient minimization could lead to unphysical values that need to be chopped, (ii) S is highly nonlinear, and simple gradient search is not efficient. An interesting property of S is that its Hessian is diagonal, therefore the single pixel approximation can be used¹⁴.

IV. NUMERICAL SIMULATION

We tried all the above mentioned deconvolution methods on a test system with two Gaussian charge distributions. The error metric we used was the difference between the original hologram and the hologram simulated from the new charge density distribution. Van Cittert and ML methods with single or double pixel approximation have shown that the convergence is very good (less than 10 iterations are necessary for convergence). However the number of electrons used to fit the data was one order of magnitude bigger than that of the original image. Tests using the Lucy-Richardson method have shown bad convergence, further studies needs to be done, but one of the reasons could be some divergence caused by the denominator in equation (5).

At this point we turned to the maximum entropy method. As we already developed the ML algorithm with single and double pixel approximation, we could easily apply the algorithm developed by Cornwell and Evans¹⁴. This algorithm tries to maximize the likelihood, the entropy and uses Lagrange multipliers to keep a constant number of electrons. Several tests have shown that the algorithm (at least the one adapted by us) was not able to minimize Q , S and F at the same time. However we found that the maximum likelihood and minimum number of electrons produces a good quality reconstruction, with improved resolution, and a reasonably good F ¹⁶. The following example was obtained using the last algorithm on a simulated hologram from a cluster of atoms.

We simulated the hologram produced by a CdTe cluster of 1000 atoms at 8 and 9 keV. We introduced a randomly distributed noise level of 10^{-3} on every data point, on a solid angle with azimuth varying from 0 to 360 degrees, the polar angle from 0 (perpendicular to the 001 direction) to 80 degrees, with 1 degree step size in each direction. Since we are interested in imaging the first neighbors, we used a smoothed hologram with 2 degrees in every direction.

The holograms generated by this charge after smoothing are shown in Fig. 1. We choose the first step to

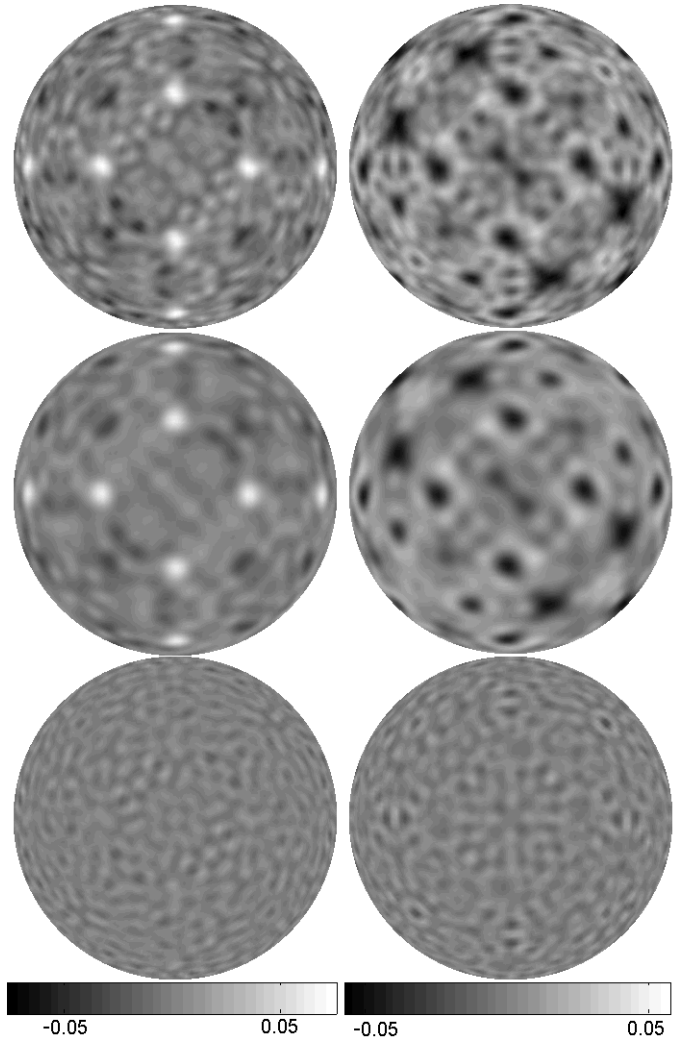


FIG. 1: (top) simulated hologram from a cluster of 1000 atoms at 8 (left) and 9 (right) keV after smoothing. (Center) Hologram generated by the fitted charge density distribution. (Bottom) Difference between top and center.

be the standard holographic reconstruction. Comparison between the standard reconstruction and the deconvolved image are shown in Figure 2.

The number of electrons within the reconstructed region is $F = 6 \cdot 10^3$ in the original picture, $F = 7 \cdot 10^4$ in the standard reconstruction, and $F = 3 \cdot 10^4$ in the deconvolved image, a factor of 5 bigger than the original image, but a factor of 2 better than the standard reconstruction. The peaks height of the charge density in the three images goes in the opposite direction, the maximum number of electrons in one voxel in the original image is 50, 0.38 in the standard reconstruction, and 14 in the deconvolved image as shown in the colorbars of Figure 3. The reason for this is that in the original image, every electron of one atom is concentrated in a single voxel, while the standard reconstruction has many electrons spread over many more voxels. The deconvolved image has a total of less electrons than the standard im-

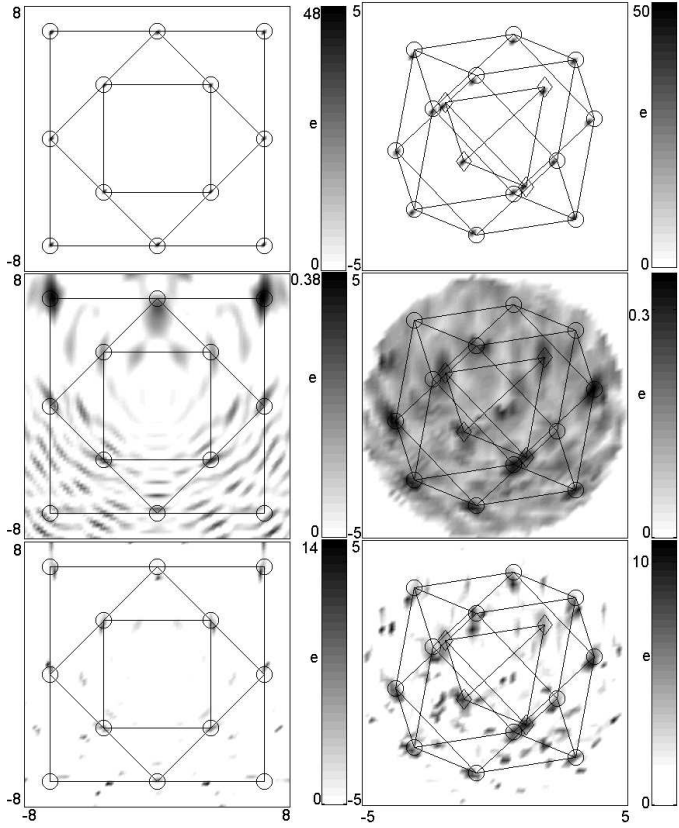


FIG. 2: (Top) original charge distribution - XZ plane (left), 3D (right). (Center) Standard holographic reconstruction. (Bottom) Deconvolved charge density distribution. The colorbar shows the maximum and minimum value. The 3D images are obtained by maximum voxel (volume-pixels) projection: the 3D matrix is rotated with respect to a plane (screen). On every pixel of the screen we project the maximum value of the voxels on top of the pixel itself.

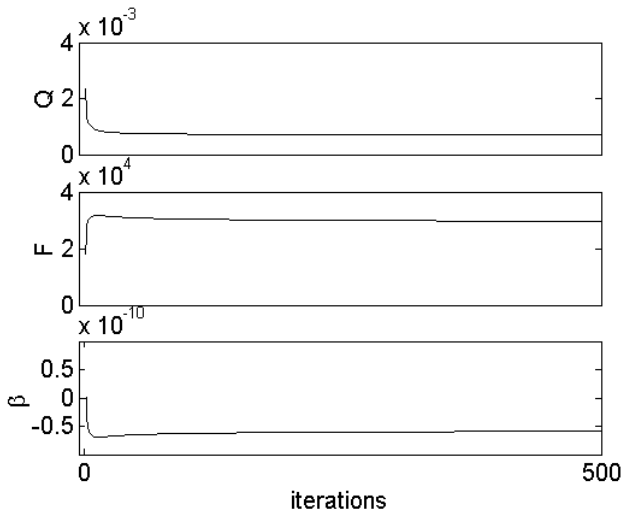


FIG. 3: behavior of the fit (Q) normalized to the volume in k -space, the number of electrons (F) and the Lagrange multiplier β . The fit is obtained quickly, while F decreases much slower.

age, but much higher peaks, due to the super-resolution. The maximum likelihood is obtained within the first 10-20 iterations (Fig. 3), dropping Q by more than a factor of 2 with respect to the standard holographic reconstruction. Notice that the hologram (Figure 2) is fitted well in the low frequency range, as we used a charge density distribution to up to 8 Å max. The residual is only at high frequency. The total number of electrons is slowly reduced in the following ~ 500 iterations.

In conclusion we would like to point out future possibilities. In this work we have demonstrated that iterative deconvolution can be applied to XFH imaging, improving the quality of the images, using many approximations. We approximated the scattering factor of an electron to be isotropic, neglecting the angular dependence of the Thompson scattering and near field effects, and we approximated the Hessian to be a sparse matrix where only the two diagonals non-zero. The storage and calculation of the full Hessian requires computers that will be available as desktop in several years. The gradient was also calculated neglecting the angular dependence of the scattering factor. Using these approximations every iteration involving the calculation of a hologram from a matrix of 80^3 voxels and the reconstruction required about 5 minutes on a Pentium II computer, for a total of one night of calculation. This image deconvolution has been obtained by enforcing a real and positive charge density distribution. Obviously once the image is deconvolved; one can use the ‘atomicity’: place atoms in the location of the peaks, and perform an optimization using the full angular dependence of the scattering factor, adjusting the atomic number and position of these atoms.

We would like to acknowledge A. Szöke and F. J. García de Abajo for fruitful discussions. This work was supported by DOE...

APPENDIX A: CALCULATION OF THE HESSIAN AND THE GRADIENT

The Hessian does not need to be known in great detail. It can be pre-calculated neglecting the angular dependence of Thompson scattering factor $\frac{f_T}{r_e} = \frac{1+\cos^2 \Theta_{\mathbf{k},\mathbf{r}}}{2}$ and using the following approximation $\int \cos^2(kr - \mathbf{k} \cdot \mathbf{r}) k^2 d^2 \hat{k} \simeq \frac{1}{2} \int_s k^2 d^2 \hat{k}$ and $\int_s \sin^2(\mathbf{k} \cdot \mathbf{r}) k^2 d^2 \hat{k} \simeq \frac{1}{2} \int_s k^2 d^2 \hat{k}$ we obtain:

$$\begin{aligned}
 H_{\mathbf{r},\mathbf{r}} &= \sum_k \Delta k \int_{s(k)} \frac{r^2}{r_e^2} \cos^2(kr - \mathbf{k} \cdot \mathbf{r}) k^2 d^2 \hat{k}, \\
 &\simeq \frac{r^2}{r_e^2} \frac{1}{2} \sum_k \Omega_k \Delta k \\
 H_{\mathbf{r},-\mathbf{r}} &= \sum_k \Delta k \int_{s(k)} \frac{r}{r_e} \cos(kr - \mathbf{k} \cdot \mathbf{r}) \cdot \\
 &\quad \cos(kr + \mathbf{k} \cdot \mathbf{r}) k^2 d^2 \hat{k} \\
 &= \frac{r^2}{r_e^2} \sum_k \Delta k \int_{s(k)} [\cos^2(kr) - \sin^2(\mathbf{k} \cdot \mathbf{r})] k^2 d^2 \hat{k},
 \end{aligned}$$

$$\begin{aligned} &\simeq \frac{r_e^2}{r_e^2} \sum_k [\cos^2(kr) - \frac{1}{2}] \Omega_k \Delta k \\ &\simeq \frac{1}{2} \frac{r_e^2}{r_e^2} \sum_k \cos(2kr) \Omega_k \Delta k \end{aligned} \quad (\text{A1})$$

where $\Omega_k = k^2 \int_{s(k)} d^2 \hat{k}$, \hat{k} is a unit vector, and $s(k)$ is the region where the hologram is measured at a given energy.

The gradient is calculated by simulating the hologram $\chi^{\{n\}}(\mathbf{k})$ generated by a charge density distribution $\rho^{\{n\}}(\mathbf{r})$, and propagating the hologram to the real space. Using $\bar{U}(\mathbf{r}) = \left(\frac{r}{r_e}\right)^2 U(\mathbf{r})$, eq. (7) can be written as:

$$\begin{aligned} \nabla Q &= 2 \left[\bar{U}^{\{n\}}(\mathbf{r}) - \bar{U}(\mathbf{r}) \right], \\ \bar{U}^{\{n\}}(\mathbf{r}) &= \eta^\dagger(\mathbf{r}, \mathbf{k}) * \chi^{\{n\}}(\mathbf{k}) \\ &\simeq 2\text{Re} \int_s \frac{r}{r_e} e^{-i(kr - \mathbf{k} \cdot \mathbf{r})} \chi^{\{n\}}(\mathbf{k}) d^3 \mathbf{k} \\ \chi^{\{n\}}(\mathbf{k}) &= \eta(\mathbf{k}, \mathbf{r}) * \rho^{\{n\}}(\mathbf{r}) . \\ &\simeq 2\text{Re} \int \frac{r}{r_e} e^{i(kr - \mathbf{k} \cdot \mathbf{r})} \rho^{\{n\}}(\mathbf{r}) d^3 \mathbf{r} \end{aligned} \quad (\text{A2})$$

These calculations can be very long as we need to sum over $\mathbf{r}(x, y, z)$ for every $\mathbf{k}(k, \vartheta, \varphi)$. Supposing that the number of points in $x, y, z, \vartheta, \varphi$ is $N \sim 100$ for every variable, we need to calculate the product in the integral of eq. (A2) for every possible value, i.e. N^5 products and sums. The computation of $\chi^{\{n\}}(\mathbf{k})$ can be performed faster if we separate the sum over the variables x, y, z .

We begin by calculating $\xi^{\{n\}}(\mathbf{r}) = \frac{r}{r_e} e^{ikr} \rho^{\{n\}}(\mathbf{r}) \Delta r^3$; we can express Eq (A2) as:

$$\chi_n(\mathbf{k}) \simeq 2\text{Re} \sum_{\mathbf{r}} e^{i\mathbf{k} \cdot \mathbf{r}} \xi^{\{n\}}(\mathbf{r}) \quad (\text{A3})$$

which is a simple Fourier transform. However the holograms are usually measured in spherical coordinates, and to obtain the values of $\chi^{\{n\}}(\mathbf{k})$ in the measured positions, we either need to perform an interpolation, or a convolution. Another approach is to use directly the spherical coordinates in the kernel:

$$\begin{aligned} e^{i\mathbf{k} \cdot \mathbf{r}} &= e^{ikx \sin \vartheta \cos \varphi} e^{iky \sin \vartheta \sin \varphi} e^{ikz \cos \vartheta} \\ &= A_{k,x,\vartheta,\varphi} B_{k,y,\vartheta,\varphi} C_{k,z,\vartheta} \end{aligned} \quad (\text{A4})$$

and Eq. (A3) becomes:

$$\begin{aligned} \chi^{\{n\}}(k, \vartheta, \varphi) &\simeq 2\text{Re} \sum_x A_{k,x,\vartheta,\varphi} \sum_y B_{k,y,\vartheta,\varphi} \cdot \\ &\quad \sum_z C_{k,z,\vartheta} \xi^{\{n\}}(x, y, z) \end{aligned} \quad (\text{A5})$$

Each sum requires N^4 calculation, reducing the time to perform the calculation by $\sim N/3$. The same trick can be applied for the holographic reconstruction.

¹ A. Szöke, AIP Conf. Proc. **147**, 361 (ed. by D.T. Attwood and J. Boker, AIP, New York, NY, 1986).
² M. Tegze, G. Faigel, Nature **380**, 49 (1996).
³ T. Gog et al. Phys. Rev. Lett. **76**, 3132 (1996).
⁴ R. Fitzgerald, Physics Today **54**, 21-3 (2000).
⁵ P. H. Van Cittert, Z. Physik **69** (1931) 298. For a more modern and English reference see *e. g.* P. A. Jansson, JOSA **60**(2), (1970), 184-191
⁶ L. B. Lucy, Astronomical Journal **79**(6), (1974), 745-54
⁷ W. H. Richardson, JOSA **62**(1), (1972), 55-59
⁸ G. Faigel, M. Tegze, Reports on Progress in Physics **62**, 355 (1999).
⁹ B. P. Tonner, Z.-L. Han, G. R. Harp, and D. K. Saldin, Phys. Rev. B **43**, 14423 (1991)

¹⁰ J. Miao et al., Nature (London) **400**, 342 (1999).
¹¹ R. W. Gerchberg, W. O. Saxton, Optik **35**, 237 (1972).
¹² J. Fienup, Appl. Opt. **21**, 2758 (1982).
¹³ S. W. Wilkins, J. N. Varghese and M. S. Lehmann, Acta Cryst A**39**, (1983) 47-60
¹⁴ T. J. Cornwell, K. F. Evans, Astronomy and Astrophysics **143**, (1985), 77-83
¹⁵ A. Szoke, Acta Cryst. A**49**, (1993), 853-866.
¹⁶ S. Marchesini, C. S. Fadley, M. R. Howells, presented at “New Approaches to the Phase Problem for Non-Periodic Objects”, May 17-19, 2001, Lawrence Berkeley National Laboratory.